BOLETIN DE LA SOCIEDAD ESPAÑOLA DE
Cerámica y Vidrio
www.elsevier.es/bsecv

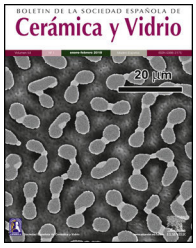

New glass-ceramic from ternary–quaternary mixtures based on Colombian industrial wastes: Blast furnace slag, cupper slag, fly ash and glass cullet

Estefania Montoya-Quesada, Mónica A. Villaquirán-Caicedo, Ruby Mejía de Gutiérrez*

Composite Materials Group, CENM, Universidad del Valle, Ciudad Universitaria Meléndez, Calle 13 # 100-00, Colombia

ARTICLE INFO

Article history:
Received 3 July 2020
Accepted 23 November 2020
Available online 1 January 2021

Keywords:
Waste management
Waste glass
Construction applications
Ceramic applications
Glass crystallization

ABSTRACT

The aim of this research was to evaluate the production of glass ceramics from novel combinations of fly ash, glass cullet, blast furnace slag and copper slag solid wastes. The CaO/SiO_2 molar ratios of the mixtures were 0.17–0.39. Glass ceramics were produced by thermal treatment of frits obtained by quenching in water. The results show that samples with a high Fe_2O_3 content (>4 wt%) are not adequate for glass-ceramic formation, as a result of the effect of ferric iron, Fe^{3+}, which increases the network connectivity, on the stability of the glass. The mechanical properties of the ceramic materials were as follows: elastic modulus of 97.8–106 GPa, Vickers microhardness of 612–701 MPa, fracture toughness of 0.45–0.84 MPa $m^{1/2}$, and friction coefficient of 0.57–1.0. For the glass ceramics, the mass loss did not exceed 1% in NaOH and 15% in HNO_3 as a result of the crystalline phases formed. The ceramic materials developed in this research could be considered for potential applications in the production of glazes for residential or industrial tiles and coatings, among others.

Nuevos materiales vitrocerámicos basados en mezclas ternarias y cuaternarias de residuos industriales colombianos: escoria siderúrgica, escoria de cobre, ceniza volante y vidrio de ventana

Palabras clave:
Manejo de residuos
Residuos de vidrios
Aplicaciones en construcción
Aplicaciones en cerámicas
Cristalización de vidrios

RESUMEN

El principal objetivo de esta investigación fue evaluar novedosas combinaciones de ceniza volante, residuos de vidrios, escoria siderúrgica y escoria de cobre combinados para la obtención de materiales vitrocerámicos. Las mezclas tuvieron una relación CaO/SiO_2 de entre 0,17-0,39. Las vitrocerámicas fueron producidas por tratamiento térmico de fritas obtenidas a partir enfriamiento en agua. Los resultados han mostrado que las mezclas con altos contenidos de Fe_2O_3 (>4% en peso) no son adecuados para la formación de vitrocerámicas.

* *Corresponding author.*
E-mail address: monica.villaquiran@correounivalle.edu.co (M.A. Villaquirán-Caicedo).
https://doi.org/10.1016/j.bsecv.2020.11.009

Estos resultados se asocian a la alta estabilidad del vidrio debido a la presencia de Fe^{3+}, el cual incrementa la conectividad y estabilidad de la estructura vítrea. Las propiedades mecánicas encontradas en los materiales vitrocerámicos fueron: módulo de elasticidad de 97,8-106 GPa, microdureza Vickers de entre 612-701 MPa, tenacidad a la fractura K_{1c} de entre 0,45-0,84 MPa.$m^{1/2}$, y coeficiente de fricción de entre 0,57-1,0. Las vitrocerámicas tuvieron una pérdida de masa no mayor al 1% en solución de NaOH y del 15% en soluciones de HNO_3. Las vitrocerámicas obtenidas en esta investigación podrían considerarse para aplicaciones potenciales como glaseados en placas domesticas e industriales y recubrimientos, entre otros.

Introduction

Glass is obtained by cooling a molten mixture of inorganic components at a certain rate or cooling certain molten rocks [1]. Most inorganic glasses can be transformed from a non-crystalline state to a crystalline state by high-temperature treatment; this process is called crystallization. In some glasses, crystallization can be controlled from thermal treatments to produce a new material that is composed of one or more crystalline phases embedded in an amorphous or vitreous matrix, giving rise to the formation of glass-ceramic materials that are generally not transparent; and has been considered since the beginning of glass production as a non-desirable defect. However, only some specific compositions are suitable precursors to these materials because some glasses are very stable and difficult to crystallize, while others crystallize very rapidly in an uncontrolled manner, resulting in unwanted microstructures [2–4]. Glass-ceramics are used in widespread fields due to their characteristics, such as chemical and mechanical durability, surface hardness, low thermal expansion coefficient, which are easily adapted to practical uses [1,5,6].

Although nature has provided essential components for the manufacture of glasses with abundant and easily removable components for centuries, synthetic chemical products and a wide range of solid waste are also used today [4]. Waste recycling has become an unavoidable requirement to optimize the use of natural resources [1,6,7]. Furthermore, by using wastes as alternative raw materials, it is possible to obtain new materials with added value and mitigate the environmental risk [6,8–10]. However, the use of waste as raw material requires strict control over the chemical composition, since the mixtures must contain the typical components of stable glasses, in particular Si and Al oxides and nucleating agents that favor crystallization. In this way, each residue must contribute an appropriate amount of vitrifying agents such as SiO_2 and Al_2O_3, as well as elements that modify and promote fusion (Na_2O, K_2O), in addition to stabilizing agents such as CaO and MgO, which are the components that give rise to glasses with adequate or special characteristics [8,11].

In general, the production of glass ceramics is carried out in a two-stage process that involves obtaining by a fusing-cooling technique at high temperatures (1100–1600 °C); then, the annealed glass, or milled frit, is heated again at a specified temperature so that partial crystallization occurs [4,12]. During this process, the shape of the original glass can be conserved by traditional glass shaping methods (the glass-ceramic process), or the shape of a mixture of molten raw materials can be conserved by crystalizing the melt by gradual cooling (petrurgic process) or sintering while crystalizing the original glass in the form of frit (sintering). In each of these processes, which are cost-effective at the industrial scale, materials can be obtained that range from transparent to opaque and that are colored or colorless, and with the appropriate composition and microstructure. The main advantage of the glass-ceramic process is that a variety of mining and industrial wastes can be incorporated in proportions of up to 100% waste after the initial vitrification itself. An important group consists of silicate-type wastes, including ashes, slags and recycled glass powder, which can be made inert and/or become new products with optimized properties, allowing them to compete with current materials in various applications [13,14]. Co-processing from secondary materials usually requires less energy and produces less pollution than the production of equivalent amounts of natural raw materials [2]. The vitrification process results in stabilization of and reduction in the volume of waste between 20% and 97% depending on the nature of the waste, thereby adding value to the waste [5]. The versatility of glass-ceramic production from industrial waste has been reported in different investigations, and a variety of solid wastes have been used: metallurgical slags [9,15–18], fly ash [19–24], glass cullet waste [25], sugarcane bagasse ash [26], copper residues [9,27] and others.

It is estimated that 40% of the energy generated in the world is from coal burning, which is equivalent to 7.7 million tons of coal consumed annually [28]. According to [29], in Colombia, the most important thermoelectric companies (Termozipa, Termopaipa and Termosochagota) generate approximately 600 kt/year of solid waste from the burning of mineral coal, better known as fly ash, which is rich in silica and alumina. On the other hand, in 2012, the steel production in Colombia was estimated to be 1.3 million tons [30], and according to [31], each ton of steel produces approximately 20% by mass of waste known as ground granulated blast furnace slag (GBFS). It is estimated that 250 million tons of GBFS are produced annually in the world [32]. GBFS is mainly characterized by high calcium oxide contents and is normally used in the Portland cement industry. Glass cullet waste, on the other hand, is a 100% recyclable material rich in silica and with considerable amounts of Na_2O (a fluxing agent); there is no clear statistical information on the total amount of glass cullet waste

generated globally, but 7% of urban solid waste is estimated to correspond to glass waste [33].

Dávalos et al. [5] studied the production of glass ceramics from mixtures of fly ash with rice husk ash and soda. The glass ceramics had good mechanical properties: a Vickers hardness of 600 MPa, modulus of elasticity of 96 GPa, and fracture toughness of 0.39–0.59 MPa $m^{1/2}$. Additionally, the materials presented good chemical durability, with a mass loss of 0.5 mg/cm^2, making them good candidates for applications in the construction sector. Barbieri [34] mixed fly ash with floating dolomite to obtain amorphous glasses at 1550 °C, and after subsequent recrystallization of this glass, partially crystallized materials were obtained. Both the original glass and the glass ceramic showed better thermal and mechanical properties than conventional glass or commercial glass ceramic. According to [35], it is possible to adjust the composition of a slag through treatment by carbon reduction to reduce iron oxides in the molten slag and through the addition of modifiers such as fly ash or tailings. In some cases, it is necessary to add nucleating agents to promote crystallization in glass. Das et al. [36] developed glass ceramics from GBFS and evaluated the effect of three separate nucleating agents, TiO_2, ZrO_2, and P_2O_5, in a proportion of 4% by weight each. The results showed that the GBFS can be converted to glass ceramic with gehlenite and mellite being the main crystalline phase detected. Refs. [37,38] successfully decreased the iron content in slag by heat treatment and managed to produce glass-ceramics by mixing copper slag with other industrial waste or sand, but this resulted in a low utilization rate of the copper slag in the production of the glass or the glass ceramic. Ref. [27] synthesized glass ceramics from copper slag, but due to the high iron content (41.55%), the authors chose to separate the glass ceramics from the slag during melting of the mixture by incorporating coke to reduce iron ions; finally, light-colored glass ceramics were produced.

According to a literature review, the use of binary or ternary mixtures of solid wastes for the production of glass and glass ceramics is limited to a few studies [5,15,19,20,24,34,39], and most studies have been based on the use of a single type of waste. The goal of the present study is to evaluate the potential of different ternary and quaternary mixtures of solid wastes from Colombia, such as fly ashes, blast furnace slag, copper slag and glass cullet waste, as raw materials for obtaining glass ceramics through controlled crystallization of frits by powder pressing and without additives. The influence of secondary and ternary systems on the microstructure, mechanical and physical properties, and chemical resistance of glass and glass ceramics were analyzed.

Materials and methods

Characterization of the raw material

The solid wastes used as raw material for the manufacturing of glass were fly ash (FA) from a boiler at the brick company Lago Verde, granulated blast furnace slag (GBFS) from Acerías Paz de Río, copper slag (ECU) from Cobres de Colombia and glass cullet (WC). The synthesis began with homogenization of the raw materials by mechanical grinding in a ball mill for 2 h. The

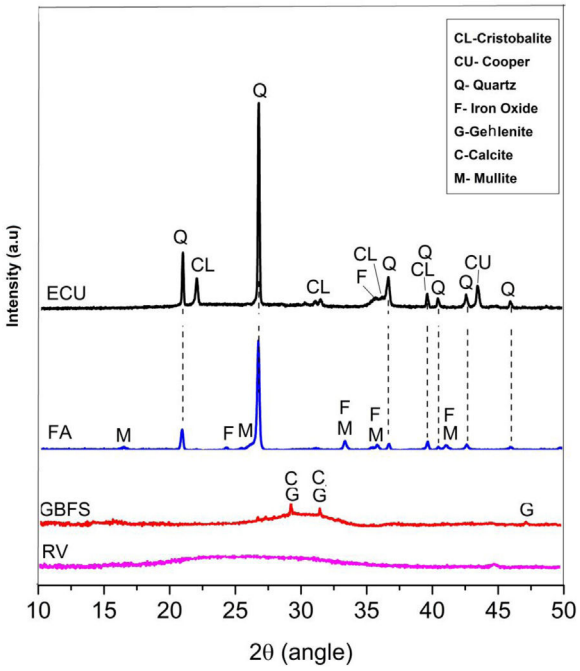

Fig. 1 – X-ray diffraction patterns of the raw materials.

chemical composition of the raw materials was determined by X-ray fluorescence (XRF) using an AXIOS MAX spectrometer (PANalytical, USA), and the powder densities were calculated by the pycnometer method according to the standards "*ASTM C329-88 Standard Test Method for Specific Gravity of Fired Ceramic Whiteware Materials*" [40]. The particle size distribution was determined using a laser particle size analyzer (Mastersizer 2000, Malvern, UK). The results are shown in Table 1.

From the XRF results, it can be observed that the solid wastes used contained significant amounts of glass network-forming oxides (SiO_2, Al_2O_3 and CaO). In addition, FA and ECU contained 4.9 and 7.73% Fe_2O_3 by weight, respectively, which can act as nucleating agents. The WC contained 13.4% Na_2O by weight, which is characterized as a fluxing agent.

The raw materials were mineralogically characterized by XRD using an X'Pert MRD PANalytical diffractometer with CuKα1 radiation generated at 20 mA and 40 kV. The specimens were scanned between 10° and 60° 2θ, with a step size of 0.02° 2θ at a speed of 4.0 s per step. The phases were identified with Crystallographica Search-Match software, supported by the Powder Diffraction File (PDF) and generated by the International Centre for Diffraction Data (ICDD). The X-ray diffraction data obtained for the wastes are shown in Fig. 1.

Fig. 1 shows that the GBFS is mainly glassy; although, there are identified peaks of gehlenite ($Ca_2Al_2SiO_7$, ICDD PDF #00-009-0216) and calcite ($Ca(CO_3)$, ICDD PDF # 01-086-2341). The WC is completely amorphous, and the FA shows signals corresponding to quartz (SiO_2, ICDD PDF # 01-084-1054) as the main crystalline phase and traces of iron oxide (Fe_2O_3, ICDD PDF #01-084-0307) and mullite ($Al(Al_{1.272}Si_{0.728}O_{4.864})$, ICDD PDF # 01-083-1881), which are common elements in these materials. Finally, two phases were identified in the ECU, corresponding to silica (SiO_2) in the form of α-quartz (ICDD PDF

Table 1 – Chemical composition, density and average particle size of raw materials.

Compounds (wt%)	FA	GBFS	WC	ECU
SiO_2	62.13	38.21	72.27	66.30
Al_2O_3	26.31	15.88	1.49	7.57
CaO	1.27	40.80	11.15	1.98
Na_2O	0.27	0.21	13.37	–
Fe_2O_3	4.88	1.87	0.62	7.75
ZnO	0.01	–	–	1.58
K_2O	0.81	0.40	0.52	0.29
CuO	0.01	–	–	13.31
TiO_2	1.19	0.51	0.08	0.25
NiO	0.01	–	–	0.02
MgO	0.25	1.32	0.26	0.33
P_2O_5	1.18	–	–	0.24
LOI[a] at 1000 °C (%)	1.02	–	–	0.24
Density (kg/m^3)	2480	2920	2488	2822
Particle average size (μm)	43.65	26.44	42.43	42.71

[a] LOI: loss on ignition.

#01-086-1560) and α-cristobalite (ICDD PDF #01-071-0785), in addition to copper in its metallic state (Cu, ICDD PDF # 00-003-1005).

Experimental design

The doses for obtaining the frits and glass ceramic were determined based on the CaO/SiO_2 molar ratio, for which mixtures with ratios between 0.17 and 0.39 were prepared by varying the percentages of the incorporated solid wastes (Table 2). This range was selected on the basis of that reported by Yang et al. [9], who claim that it is the most appropriate range for the crystallization process. The materials produced were identified with the codes F (frit), G (glass) and GC (glass ceramic), followed by the CaO/SiO_2 ratio used. Table 3 shows the theoretical chemical compositions estimated for glasses described in Tables 1 and 2.

Shi et al. [41] claimed that the glass ceramics of the $CaO–Al_2O_3–SiO_2$ (CAS) system do not have a price advantage compared decorating materials in constructions due to the high cost of the required materials. However, the use of solid wastes with a demonstrated ability to yield CAS glass ceramics with adequate properties, as reported by different authors [41–44], will increase their application in the construction sector.

Production of frits, glasses and glass ceramics

Fig. 2 outlines the general scheme for the synthesis of frits, glasses and glass ceramics. Powders of the raw materials were homogenized and melted in an alumina crucible at 1450 °C in an electric furnace (Nabertherm, Germany) for 2 h to remove any crystalline phase. The melted materials were rapidly poured into a water bath (quenched) at a room temperature of 25 °C to obtain the frits. The frits were ground into a fine powder in a mortar until a particle size smaller than 75 μm (sieve no. 200) was obtained. Then, the frits were characterized by differential scanning calorimetry (DSC) to determine the glass transition temperature (T_g) and the possible temperature at which they crystallize (T_p).

To obtain glasses and glass ceramics from the thermal treatment of glass powders, the ground frit powder was mixed with approximately 10 wt% H_2O, compacted and pressed at a pressure of 8–9 tons using a PIKE Technologies Crush IR manual hydraulic press until pellets with a diameter of 13 mm and a height of 3 mm were obtained. For glasses, the compacted samples were annealed at a temperature close to the glass transition temperature (T_g) in an electric furnace. The choice of performing the treatments at temperatures close to T_g was based on the results reported by Takahashi et al. [45] for CAS glasses obtained from high-purity commercial powders. For glass ceramics, the compacted frit samples were thermally treated in an electric furnace from room temperature to T_p. A holding time of 2 h was maintained for both processes, and the heating rate was 10 °C/min. Then, the samples were removed from the furnace and cooled to room temperature.

Characterization of glasses and glass ceramics

- DSC thermal analyses were carried out in an SDT Q-600 thermobalance (TA Instruments); the samples were placed in an alumina crucible; the air flow was 100 mL min^{-1}, and the heating rate was 10 °C/min.
- The samples were characterized as KBr pellets by Fourier transform infrared (FTIR) spectroscopy on a PerkinElmer Spectrum 100 spectrometer. The spectra were collected at a room temperature of 25 °C over a wavenumber range of 4000–400 cm^{-1}.
- The mineralogical composition of the samples was determined using an X'Pert MRD PANalytical diffractometer with CuKα radiation generated at 45 kV and 40 mA; the specimens were scanned between 10 and 60° 2θ with a step size of 0.02°. The crystalline phases of the glass-ceramic precursor glasses were identified using Crystallographica Search-Match software.

Table 2 – Proportion by weight of solid wastes used to obtain frits with different CaO/SiO_2 molar ratios.

Sample ID	CaO/SiO_2 molar ratio	Proportion (wt%)			
		FA	WC	GBFS	ECU
0.17	0.17	0.40	–	0.20	0.40
0.24	0.24	0.30	0.50	0.20	–
0.27	0.27	0.20	0.10	0.30	0.40
0.36	0.36	0.50	0.10	0.40	–
0.37	0.37	–	0.20	0.40	0.40
0.39	0.39	0.30	0.30	0.40	–

Table 3 – Theoretical chemical composition estimated for the designed frits.

Compounds (wt%)	Frits.					
	0.17	0.24	0.27	0.36	0.37	0.39
SiO_2	59.01	62.42	57.64	53.58	56.26	55.60
Al_2O_3	16.73	11.81	13.20	19.66	9.68	14.69
CaO	9.46	14.12	14.40	18.07	19.34	20.05
Na_2O	0.15	6.81	1.45	1.56	2.76	4.18
Fe_2O_3	5.43	2.15	4.70	3.25	3.97	2.40
ZnO	0.64	0.00	0.63	0.01	0.63	0.00
K_2O	0.52	0.58	0.45	0.62	0.38	0.56
CuO	5.33	0.00	5.33	0.01	5.32	0.00
TiO_2	0.68	0.50	0.50	0.81	0.32	0.59
NiO	0.01	0.00	0.01	0.01	0.01	0.00
MgO	0.50	0.47	0.60	0.68	0.71	0.68
P_2O_5	0.57	0.35	0.33	0.59	0.10	0.35

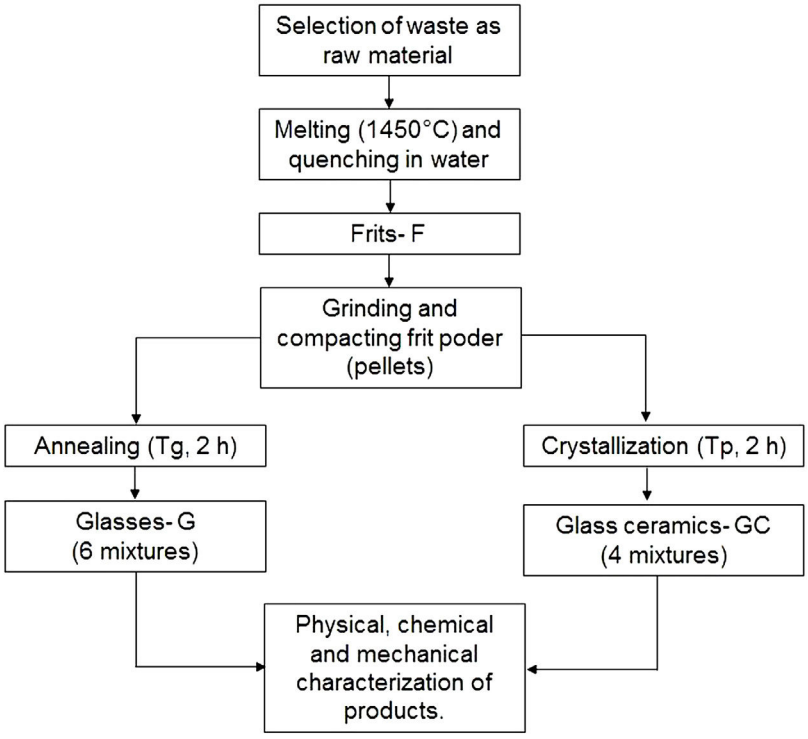

Fig. 2 – General scheme outlining the process of obtaining glasses and glass ceramics.

- Microstructural observations of the samples were performed using a JEOL JSM-6490LV scanning electron microscope in backscattered electron mode between 20 kV and 25 kV. The samples were embedded in resin, and their surfaces were roughened with abrasive paper (400, 600, 1000 and 1200 grit), polished using a cloth with colloidal silica to achieve a mirror-finished surface, washed with distilled water, dried and then coated with gold.
- The microhardness of the polished glasses and glass ceramics was determined using a ZwickRoell Indentec ZHμ

microhardness tester, which can be used for Vickers and Knoop hardness tests. A load level of 100 gf and an indentation time of 15 s were used. The Knoop hardness (H_k) indenter was applied for only the glasses because the porosity of the samples made it difficult to achieve an acceptable indentation footprint with the Vickers hardness (H_V) indenter. For glass ceramics, the Vickers indenter was used. To obtain reliable statistical data, at least six indentations were made in each sample, and average values are reported.

- The elastic modulus (E) of the glass ceramics was determined by a nanoindentation test. Nanoindentations were generated on an IBIS Authority system (Fischer–Cripps) with a Berkovich-type diamond tip in closed-loop mode. The applied load was 1 mN, and each consecutive indentation was separated by 10 μm to avoid any residual stress interference from adjacent indentations (10 indentations per sample). The mechanical properties were deconvoluted using the Oliver and Pharr method [46].
- The fracture toughness (K_{ic}) of glass ceramics was calculated using the model by Anstis et al. [47], according to Eq. (1), which is based on the length of the cracks originating from the corners of the Vickers indentations:

$$K_{ic} = 0.016\sqrt{\frac{E}{H}}\left(\frac{P}{c^{3/2}}\right) \quad (1)$$

where E is the elastic modulus of the sample; P is the indentation load in Newtons; H is the Vickers hardness in GPa, which is defined as the applied load over the projected area; and c is the crack length in meters [47].

- Wear tests were performed on the samples using a pin-on-disk tribometer (CSEM Instruments) for the determination of the friction coefficients (μ) of the materials under study, per the ASTM G99-05 standard [48]. The tests were performed at a temperature of 20 °C and a relative humidity of 50% using an alumina (Al_2O_3) ball with a diameter of 10 mm under the following conditions: a stroke length of 3 mm, frequency of 20 Hz (0.03 m s^{-1}), sliding distance of 75 m and normal applied load of 6 N.
- The linear shrinkage (LS) was calculated based on the dimensions of the untreated samples and the resulting sintered samples using Equation 2 [49]:

$$LS = \frac{D_i - D_f}{D_i} \times 100 \quad (2)$$

where D_i corresponds to the diameter of the untreated sample, and D_f is the diameter of the sample after thermal treatment.

- The physical characteristics (apparent density (ρ_a), water absorption (A_{24h}) and volume of permeable pores (V_{pp})) of the GC samples were determined according to the methods established in the ASTM C642-13 standard [50]; the porosity (P) was determined by the Archimedes principle. The chemical resistance was evaluated based on the initial and final weight difference after immersing the materials in an acidic solution (HNO_3) and an alkaline solution (NaOH) at 10% by volume and a temperature of 80 °C for exposure times of 2, 4 and 6 h.

Table 4 – Heat treatment temperatures selected for the frits based on the DSC data for the production of glasses (T_g) and glass ceramics (T_p).

Frits	T_g	Ref.	T_p
F0.17	892 + 8 °C	[45]	Unclear
F0.24	780 °C		824 °C
F0.27			Unclear
F0.36	823 °C		1008 °C
F0.37	780 °C		864 °C
F0.39	690 + 60 °C	Present work	893 °C

Results and discussion

Thermal analysis and frit crystallization

Differential scanning calorimetry (DSC) is a thermal analysis technique that measures the flow of heat into or out of a material as a function of temperature or time [51]. The DSC results for the frits are shown in Fig. 3 and were used for determining the heat treatment conditions necessary to convert a glass system into a glass ceramic with the desired crystalline phases [43]. An endothermic peak at $T < 200$ °C can be observed in all the samples (Fig. 3a) and is attributed to the removal of adsorbed water [47]. However, the T_g values in the DSC results for the frits were unclear (except for F0.39), and the temperatures selected to treat and obtain the glasses were those used in Takahashi et al. [44], as is shown in Table 3. The only frit sample presenting a slight endothermic peak at 690 °C attributed to T_g was F0.39 (Fig. 3b). Deubener et al. [52] found that in systems with very rapid crystallization upon heating, T_g can be eclipsed by exothermic crystallization.

However, glass is a metastable phase material and, with the proper thermal treatment, will form crystalline phases when heated to the crystallization temperature T_p [41]. The T_p values determined from the DSC data for crystallizing the frits are shown in Table 4. The exothermic peaks corresponding to crystallization at T_p for samples F0.24, F0.36, F0.37 and F0.39 could be identified at temperatures of 824–1008 °C. Samples F0.17 and F0.27 did not present any exothermic peaks, which indicates that these samples are very stable against crystallization [53]. Yang et al. [9] found that increases in the CaO/SiO_2 ratio decrease the crystallization temperature due to an enrichment in Ca^{2+} cations, which accelerate the destruction of the silicate network by breaking Si—O—Si bonds and creating non-bridging oxygen groups (Si—O—NBO). However, in Fig. 3, T_p does not appear to increase or decrease according to the CaO/SiO_2 ratio.

The DSC curves of samples F0.24, F0.36 and F0.37 show a single exothermic crystallization peak, which suggests the formation of a single crystalline phase after heat treatment [9]; in contrast, sample F0.39 presented two exothermic peaks, the first appearing at 801 °C and the second at 893 °C. Based on the experimental results (Fig. 3), the heat treatment temperatures for the glasses were determined; in the case of sample F0.39, the maximum T_p was selected to ensure the complete formation of the crystalline phases.

Fig. 4 shows visual appearance of the glass ceramics obtained from secondary and ternary mixtures with different

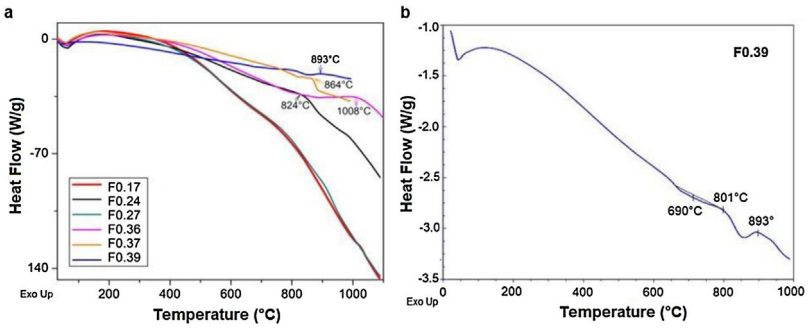

Fig. 3 – (a) DSC results for the frits and (b) magnification of the DSC curve for frit F0.39.

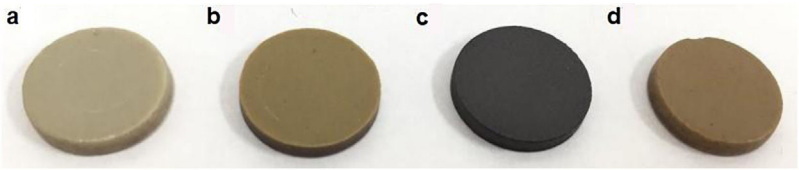

Fig. 4 – Glass ceramics obtained at T_p. (a) GC0.24, (b) GC0.36, (c) GC0.37 and (d) GC0.39.

CaO/SiO_2 ratios. Transition elements such as Cr, Cu, Ag, Mn and Fe determine the color of glass objects [54]. Of the different glass ceramics produced, the light gray color of sample GC0.24 is attributed to the proportion of glass waste in the mixture; samples GC0.36 and GC0.39 are light brown in color, which is attributed to the presence of iron [9]; and the black color of sample GC0.37 is attributed to the copper in the mixture.

FTIR spectroscopy of frits and glass ceramics

The FTIR spectra of the samples before and after sintering are shown in Fig. 5. In general, it can be observed that the frits (Fig. 5a) exhibit the same three broad bands in the mid-infrared region (1400–400 cm^{-1}) in all the obtained spectra. The broad band at 1200–800 cm^{-1} is assigned to stretching vibrations of the Si—O—Si bonds in the tetrahedral unit [SiO_4]; the band at 550–450 cm^{-1} corresponds to bending vibrations of Si—O—Si and Si—O—Al bonds [9,41]. The bands located in the 800–620 cm^{-1} region are attributed to symmetric stretching vibrations of the tetrahedral structure, including TOT (T = Si, Fe, Al), which indicates an aggregated structure of the glass. According to [43], the presence of absorption bands in the FTIR spectra of the frits (Fig. 5a) indicates that the produced materials are not completely amorphous. However, the CaO/SiO_2 ratio does not seem to affect the nature of the acquired spectra, and the differences observed in the spectra could be related to the degree of depolarization of the glass structure [9,43].

The FTIR spectra of the glass ceramics are presented in Fig. 5b. Compared to the frits, crystallization is evident in the heat-treated samples, as indicated by the formation of new bands in the 1200–800 cm^{-1} and 665–508 cm^{-1} regions, highlighting the deterioration of the silica network and the formation of new crystal phases after heat treatment. The main band for GC0.39 is shifted left toward higher wavenumbers (999 cm^{-1}) with respect to the starting frit (981 cm^{-1}). In the case of GC0.24, the band is shifted toward lower wavenumbers (1015 cm^{-1}), whereas in samples GC0.36 and GC0.37, there are new bands at 1077, 1016, 1015, 950 and 947 cm^{-1}, which could be attributed to the presence of the wollastonite crystalline phase. The presence of this phase is corroborated by XRD (explained later) and has also been identified by other authors [41]. The heat treatment leads to glass crystallization, which induces new bands located in the 820–655 cm^{-1} and 665–508 cm^{-1} regions, which are associated with M—O stretching vibrations, where M = Si or Al, and O—Si—O bending vibrations, respectively [41]. Finally, the band between 508 and 450 cm^{-1} is attributed to the bending stretching of O—Si—O and O—Al—O groups and the stretching of Ca—O groups [9,55].

Analysis of the formation of glass ceramics

As mentioned above, in frits F0.17 and F0.27, no crystallization temperature was observed in the DSC data (Fig. 3). According to the theoretical chemical compositions (Table 3), this can be related to the high content of Fe_2O_3 from the raw materials (ECU and FA), which result in iron contents of approximately 5.43 wt% and 4.70 wt%, respectively, in mixtures G0.17 and G0.27. Yang et al. [7] found that the residual iron in glass is oxidized to Fe^{3+} during the melting of glass. Furthermore, the intermediate behavior of iron(III) (Fe^{3+}) can stabilize the glass, reducing the crystallization ability and increasing the connectivity of the network [9]. In Fig. 6, the X-ray diffraction patterns of glasses G0.17 and G0.27 reveal the completely amorphous nature of these glasses.

The X-ray diffraction patterns of the obtained glass ceramics are shown in Fig. 7. For samples GC0.24, GC0.36, GC0.37 and GC0.39, different crystalline phases, mainly from the plagioclase group, such as anorthite, anorthoclase and labradorite, were identified. Sample GC0.24 contained ordered sodium anorthite ((Ca, Na) $(Al, Si)_2$ Si_2O_8, ICDD PDF #20-528), anorthoclase ($Na_{0.71}K_{0.29}AlSi_3O_8$, ICDD PDF

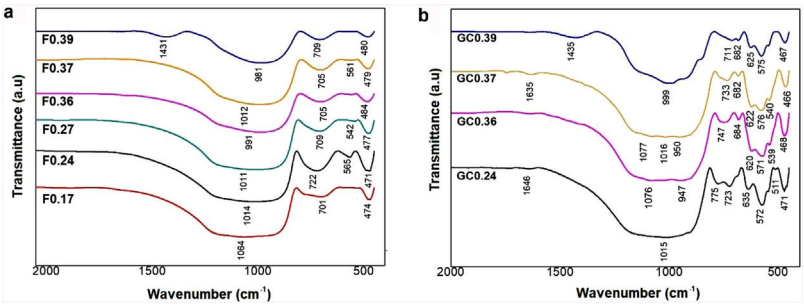

Fig. 5 – FTIR spectra of the (a) frits and (b) glass ceramics.

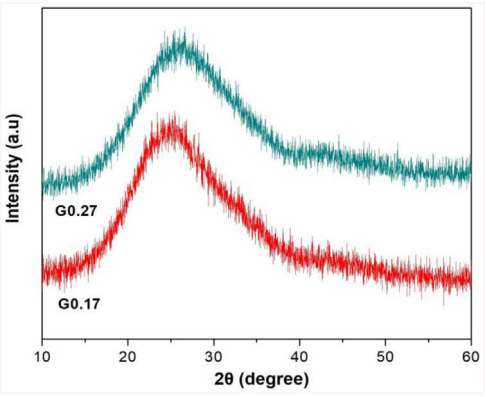

Fig. 6 – X-ray diffraction patterns of glasses G0.17 and G0.27.

#10-361) and wollastonite ($CaSiO_3$, ICDD PDF #75-1396). In sample GC0.36, many crystalline phases, such as anorthite ($CaAl_2Si_2O_8$, ICDD PDF #41-1486), albite ($Na(AlSi_3O_8)$, ICDD PDF #20-548), wollastonite ($CaSiO_3$, ICDD PDF #83-2198) and labradorite ($Na_{0.45}Ca_{0.55}Al_{1.55}Si_{2.45}O_8$, ICDD PDF #78-434), were observed. Sample G0.37 contained Haüyne ($(Na, Ca)_8$ $(Si, Al)_{12}$ O_{24} $(SO_4)_2$, ICDD PDF #20-1087); labradorite ($(Na_{0.4}Ca_{0.6})Al_{1.6}Si_{2.4}O_8$, ICDD PDF #3-499); albite ($Na(AlSi_3O_8)$, ICDD PDF #20-548), which overlapped with some of the peaks of the labradorite phase; and wollastonite ($CaSiO_3$, ICDD PDF #10-489). Finally, sample GC0.39 contained ordered sodium anorthite ((Ca, Na) $(Al, Si)_2$ Si_2O_8, ICDD PDF #20-528), akermanite ($(Ca_{1.53}Na_{0.51})(Mg_{0.39}Al_{0.41}Fe_{0.16})Si_2O_7$, ICDD PDF #72-2127) and Haüyne ($Na_6Ca_2Al_6Si_6O_{24}$ $(SO_4)_2$, ICDD PDF #73-1920).

The coexistence of multiple crystalline phases reflects the complexity and uncertainty of crystallization in the CAS glass system [41], although varying the CaO/SiO_2 ratio did not drastically influence the type of crystalline phases formed in the mixtures. As shown in Fig. 7, anorthite was the main crystalline phase in samples GC0.24, GC0.36 and GC0.39, whereas in sample GC0.37, the main crystalline phase was labradorite; however, labradorite is considered to consist of a variety of anorthite phases. Anorthite and labradorite belong to the plagioclase family; however, labradorite corresponds to the group of sodium and calcium plagioclases, whereas anorthite corresponds to the group of calcium plagioclases [56]. The formation of akermanite was observed in only GC0.39; this coincides with the DSC data, showing two exothermic peaks

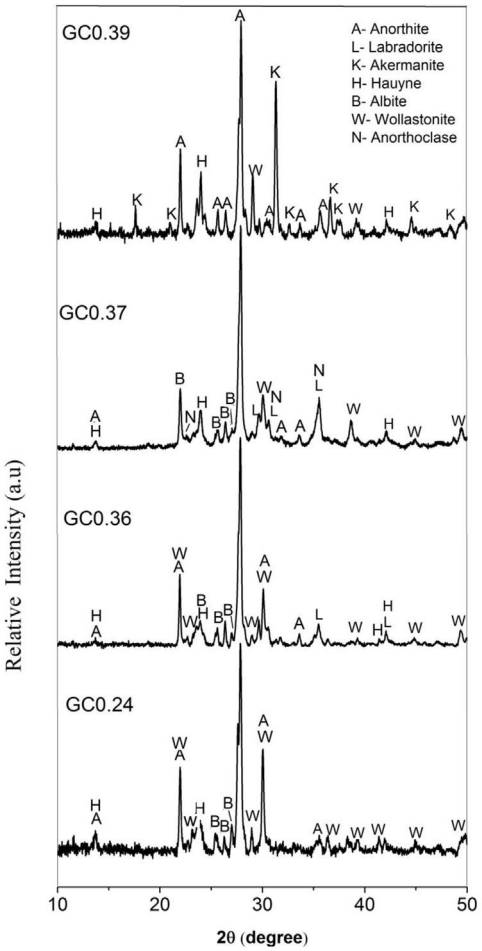

Fig. 7 – X-ray diffraction patterns of glass ceramics GC0.24, GC0.36, GC0.37 and GC0.39.

associated with two main crystalline phases and the peak at 801 °C corresponding to akermanite [57,58].

To confirm the DSC and XRD results and to obtain more information on the crystallization mechanism and microstructure, scanning electron microscopy (SEM) was performed on a polished section of the samples. Fig. 8 shows micrographs of the glass-ceramic (Fig. 8a–e) and glass (Fig. 8f) microstructures. The glass ceramics have a dense structure containing pores and a residual glassy phase, which are common in most glass ceramics due to the partial crystallization

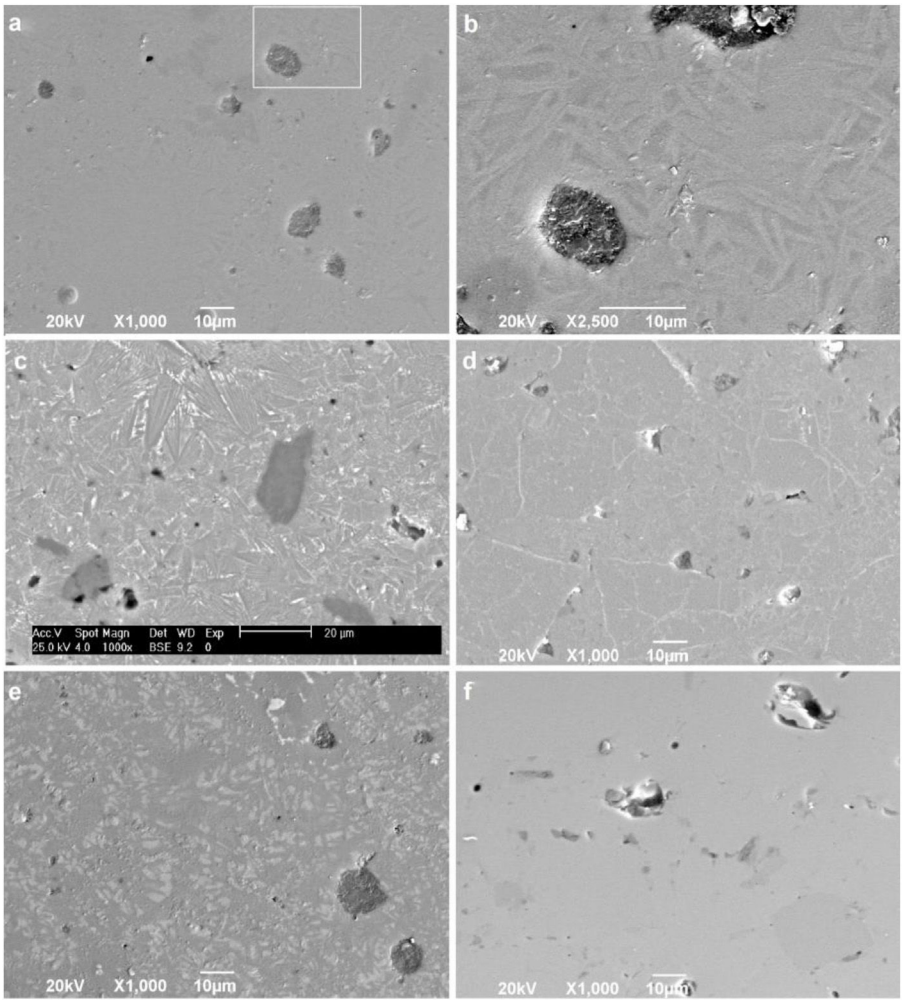

Fig. 8 – Morphology of glass ceramics. SEM images of (a) GC0.24, (b) GC0.24 (zoom), (c) GC0.36, (d) GC0.37, (e) GC0.39, and (f) the glass G0.39.

of the original glass; however, the size and shape of the grains are different for each sample. Due to the direction and growth of the crystals in samples GC0.24, GC0.36 and GC0.39, it can be assumed that crystallization occurs at the surface, given that crystallization is observed toward the interior of the glassy matrix [57]; this behavior was not as evident in sample GC0.37.

Fig. 8b is an enlarged section of Fig. 8a, and the formation of needle-like structures dispersed on the matrix is better observed; however, the glassy phase was more extensive in samples GC0.36 and GC0.39. Crystals of various sizes and morphologies are observed in Fig. 8c: a microstructure with randomly distributed dendritic pyroxene, which could be attributed to wollastonite [59]; a needle-like structure characteristic of anorthite and albite in the form of irregular plates; and the presence of irregular crystals of a darker tone dispersed in the matrix, which can be associated with the presence of Fe in the samples [4,19,55].

In Fig. 8d, white branching uniformly distributed along the matrix was observed, which according to [60], is associated with the texture of plagioclases. In glass ceramic GC0.39 (Fig. 8e), the presence of lighter-toned, irregularly distributed crystals is observed throughout the entire matrix. Comparing GC0.39 with its precursor glass G0.39 (Fig. 8f) reveals that GC0.39 has a glassy phase microstructure; no crystals are observed, but there are open and closed pores.

Evaluation of physical and mechanical properties

Table 5 shows the physical and mechanical properties of the glasses and glass ceramics under study. The density (ρ) of the annealed glasses was between 2313 and 2570 kg/m^3, whereas that of the glass ceramics was between 2528 and 2620 kg/m^3. According to [61], the density of glass depends on the molecular weight, oxide content and compactness of the glass network, whereas the density of glass ceramics depends mainly on the crystalline phases formed. As expected, the density of the glass ceramics was higher than the density of the annealed glass for each pair, which reflects the fact that the molar volume of a glass ceramic has to be lower than that of the corresponding glass, given that the general composition is the same [61]. Glass ceramics GC0.37 and GC0.39 have slightly higher densities than the glasses of the same composition, which can be associated with the fact that GC0.37 and GC0.39 contain phases such as akermanite, which are slightly

Table 5 – Physical and mechanical properties of the glasses and glass ceramics produced.

Sample	Properties									
	E (GPa)	H_V (MPa)	H_k (MPa)	K_{ic} (MPa $m^{1/2}$)	μ	ρ (kg/m^3)	LS (%)	V_{pp} (%)	A_{24h} (%)	P (%)
Glasses										
G0.17	–	–	607 ± 21	–	0.47	2570 ± 5	–	5.81 ± 0.09	3.22 ± 0.25	8.23 ± 0.53
G0.24	–	–	662 ± 18	–	–	2313 ± 31	–	9.85 ± 0.13	3.27 ± 0.24	7.73 ± 0.41
G0.27	–	–	–	–	–	2409 ± 83	–	7.88 ± 0.52	4.20 ± 0.73	10.27 ± 1.58
G0.36	–	–	667 ± 21	–	0.52	2565 ± 34	–	2.11 ± 0.25	0.31 ± 0.09	1.24 ± 0.08
G0.37	–	–	620 ± 26	–	–	2524 ± 72	–	12.80 ± 0.64	4.87 ± 0.55	12.32 ± 1.00
G0.39	–	–	555 ± 16	–	–	2558 ± 23	–	1.31 ± 0.16	3.71 ± 0.72	1.24 ± 0.44
Glass ceramics										
GC0.24	97.8 ± 17.0	612 ± 36	–	0.84 ± 0.09	0.94	2528 ± 29	11.83 ± 0.80	0.46 ± 0.00	0.07 ± 0.01	0.18 ± 0.03
GC0.36	105.8 ± 10.3	632 ± 78	–	0.45 ± 0.12	0.72	2620 ± 37	11.61 ± 0.22	1.41 ± 0.65	0.29 ± 0.19	1.03 ± 0.28
GC0.37	105.9 ± 17.2	701 ± 43	–	0.99 ± 0.16	0.57	2596 ± 53	8.35 ± 0.16	9.27 ± 1.94	2.12 ± 0.17	5.71 ± 0.42
GC0.39	102.2 ± 16.4	667 ± 60	–	1.06 ± 0.04	1.00	2594 ± 50	11.29 ± 0.54	0.57 ± 0.08	0.08 ± 0.03	0.22 ± 0.07

denser than other phases (2920 kg/m^3, as calculated by the method of Appen) [58]. Phases such as diopside are denser in the crystalline state (3270 kg/m^3) than in the glassy phase (2750 kg/m^3) [58]. The results obtained for the volume of pores (V_{pp}), water absorption (A_{24h}) and porosity (P) are well correlated; these values were higher in the glasses than in the glass ceramics of equivalent composition.

The Knoop hardness (H_K) and Vickers hardness (H_V) values were determined for the glasses and glass ceramics, respectively, under the same load and indentation time. Glass samples G0.24 and G0.36 presented the highest Knoop hardness values (662 and 667 MPa, respectively) of all the glasses; the hardness of sample G0.27 is not reported in Table 4 because a load of 50 gf yielded a very low hardness of 275 MPa. In addition, according to [62], the Knoop hardness is always lower than the Vickers hardness because the Knoop indenter penetrates to approximately half the depth of the Vickers indenter. The Vickers microhardness values of the glass ceramics were 612 ± 36 and 701 ± 43 MPa, and the highest value was achieved for GC0.37. Dávalos [5] found similar Hv values (570–643 MPa) for glass ceramics from RHA and soda. Wollastonite-based glass ceramics usually have hardness values of 600 MPa [3]. Ref. [63] produced anorthite-wollastonite glass ceramics with Vickers hardness values of 540–613 MPa, and [64] produced wollastonite diopside glass ceramics with $H_{V0.5}$ hardness values of 600–650.

The porosity and hardness of the glass ceramics are listed in Table 5. According to [9,65,66], an increase in the CaO/SiO_2 ratio promotes glass crystallization, which can increase the density and hardness of a sample. However, in this study, the density and hardness first increased and then decreased as the CaO/SiO_2 ratio increased, reaching maximum values for sample GC0.37, and it was not possible to find a direct relationship between the density and CaO/SiO_2 ratio. This behavior can be associated with (i) greater pore formation in the center of the grains in GC0.39, which can interrupt the propagation of microcracks [67], and (ii) the considerable decrease in melt viscosity with the increase in the CaO/SiO_2 ratio [65], which increases the porosity. In general, the densities of the glass ceramics obtained were between 2528 ± 29 and 2620 ± 37 kg/m^3, and these values are similar to reported bulk densities for wollastonite glass ceramic [3], albite-anorthite glass ceramic [5], wollastonite-nepheline glass ceramic [66] and cristobalite-anorthite glass ceramic [68].

However, a comparison of the theoretical chemical composition of glass ceramics with that of glass (Table 3) shows that in general, a higher content of CaO and MgO and a higher elastic modulus can be obtained for glass ceramics. The H_V of glass ceramics also depends on the composition, quantity, distribution and morphology of the crystalline phases, in addition to the interaction between the crystal and residual glass, because the boundaries between the glass and the crystal and between the crystals are the weakest regions; the smaller the grain size of the crystal, the longer the path required for the propagation of cracks [1,2]. Authors such as [66,68] have found reduced hardness in glass ceramics, probably due to the internal stress generated by the high crystallinity. These results could be corroborated by the SEM images: GC0.36 (Fig. 8c) showed larger crystal grain sizes and a K_{iC} of 0.45 MPa m$^{1/2}$, whereas GC0.39 (Fig. 8e) showed smaller crystal grain sizes and a K_{iC}, of 1.06 MPa m$^{1/2}$.

The glass-ceramic materials presented a higher friction coefficient (μ) than the glasses (G0.17 and G0.36) and, therefore, would be expected to be less susceptible to surface damage that causes defects. This is associated with the fact that, in glasses, a crack is propagated in a single homogeneous phase, whereas in glass ceramics, the crack has to pass through boundaries that are the limits of different crystal phases such as albite and anorthite [69]. Fuertes et al. [70] claimed that when friction occurs in glass ceramics, the glassy phase, which generally covers the surface of the material, is removed first; then, contact with the crystals begins. This is why a larger glassy phase proportion generates more slips of both the microcrystal and the glassy phase and causes larger microcracks and deeper wear grooves as a consequence of a greater detachment of the material [70]. The friction coefficient can be affected by many factors, such as the humidity, surface roughness, hardness, fracture toughness and Young's modulus, which are influenced by characteristics of the phase composition and microstructure, such as crystal size, porosity, secondary phases or crystallinity [70]. Fuertes et al. [70] reported friction coefficient values of 0.43, 0.49 and 0.66 for albite-based glass ceramics, anorthite-based glass ceramics and a standard floor tile glaze, respectively, which are lower than the values obtained for the glass ceramics but similar to those obtained for the glasses in this study.

The linear shrinkage (LS) values for GC0.24, GC0.36 and GC0.39 (11.83, 11.61 and 11.29%, respectively) were similar, whereas sample GC0.37 produced a lower value (8.35%), which indicates a lower degree of densification. This conclusion is confirmed by the porosity assessment, where the maximum porosity (5.71%) was obtained for GC0.37. According to [67], the lower densification in GC0.37 can be attributed to a possible mass crystallization that inhibited densification and to the content of Fe_2O_3 (3.92% by weight).

The elastic modulus of a material decreases with increasing porosity [71]; however, the glass ceramics with the highest porosity reported in this study were those with the highest elastic modulus. This is explained by the fact that the elastic modulus is also determined by the degree of crystallization, the elastic constants of the main crystalline phases and the amount of residual glass phase in the material [72]. However, an effect based on the differences in equilibrium between the different crystalline phases and the consequent residual thermoelastic stresses developed when cooling cannot be excluded [73]. As can be observed in the SEM images (Fig. 8), there is a higher proportion of the glassy phase in sample GC0.24 than in the other samples, which corroborates its lowest elastic modulus (97.8 GPa). In general, the materials developed in this investigation had a higher modulus of elasticity than commercial glass ceramics, as reported by Slagsitall (70–100 GPa) and Neoparies (88 GPa); furthermore, the moduli were double the values reported for natural stones such as granite (40–60 GPa) and marble (30–50 GPa), and the fracture toughness (K_{ic}) values found in this study were similar to those reported for Neoparies (0.7 MPa m1/2), marble (0.5 MPa m1/2), some floor tile glazes (0.66–1.3 MPa m$^{1/2}$), granite (1.1 MPa m$^{1/2}$), glass

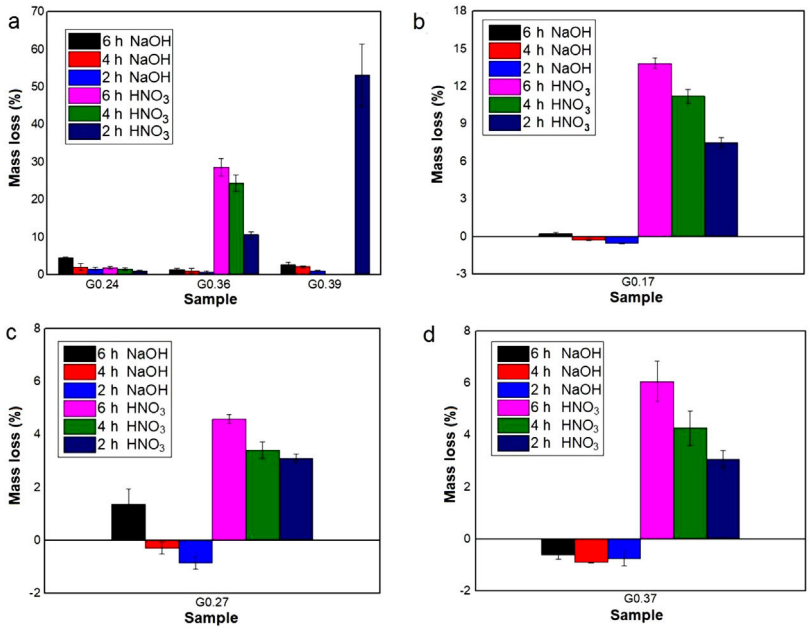

Fig. 9 – Chemical resistance of samples exposed for 2, 4 and 6 h at 80 °C to NaOH (10% vol.) and HNO_3 (10% vol.) solutions: (a) Glasses obtained from the same wastes (FA-RV-GBFS) but in different proportions (G0.24, G.036 and G0.39), (b) G0.17 (FA-GBFS-ECU), (c) G0.27 (FA-RV-GBFS-ECU) and (d) G0.37 (GBFS-RV-ECU).

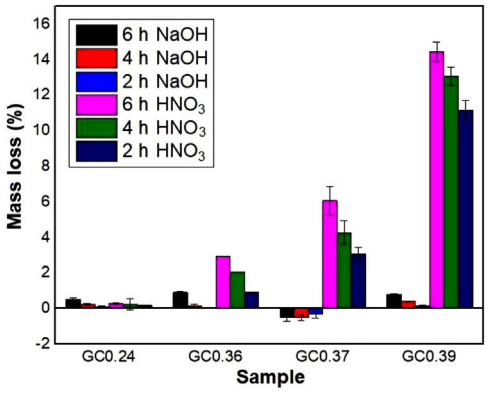

Fig. 10 – Chemical resistance in solutions of NaOH (10% vol.) and HNO_3 (10% vol.) for GC samples exposed for 2, 4 and 6 h at 80 °C.

ceramic obtained from goethite (0.6–3.0 MPa $m^{1/2}$), and coal ash and rice husk ash (0.46–0.59 MPa $m^{1/2}$) [5,6,67,70].

Evaluation of chemical resistance

Chemical resistance depends on several factors, such as the pH of the solution and test parameters such as the exposure area, time and temperature; the composition and amount of residual glass; and the amount of crystalline phases formed in the glass ceramics [74]. The chemical resistance of the glasses (Fig. 9) and glass ceramics (Fig. 10) was evaluated by immersing them in a 10% solution of NaOH and a 10% solution of HNO_3 at 80 °C for different time periods of time (2, 4 and 6 h). In general, as expected, the mass loss of the materials increased as the immersion time increased, which can be attributed to a slower release of the glass components into the solution. The mass loss of the glasses in the alkaline solution did not exceed 5% by weight, whereas in the acidic solution, the mass loss was between 4% and 26% (Fig. 9). For the glass ceramics, the mass loss did not exceed 1% in NaOH and 15% in HNO_3 as a result of the crystalline phases present (Fig. 10). In general, mass losses were higher in the presence of HNO_3 than in the presence of NaOH, which coincides with the reports of several authors [4,23,24,75] and was due to the alkaline components from the raw material (e.g., CaO, Al_2O_3 and Fe_2O_3), which have a tendency to react with strong acids [75]. In addition, all transition elements, such as Cr, Cu, Ag, Mn and Fe, act as modifiers of the glass network, and some increase the risk of deterioration [54].

Acidic solutions are characterized by the presence of H^+/H_3O^- ions, and as a consequence of the excess protons, attack takes place preferentially by ionic interdiffusion between the protons (or hydronium ions) of the medium and the alkaline cations of the glass network, which are the most weakly bonded to the glassy network and, therefore, the easiest to remove, the chemical attack leads to the depolymerisation of the glass network and the different glass ions dissolve [59]. The amount of alkaline ions extracted depends on their nature and concentration, the type of glass, the time of attack and the temperature. If the alkaline content is low, the initial acid attack improves the chemical resistance of glass against subsequent attacks because the removal of the alkaline ions gives rise to the formation of a silica-enriched layer via partial condensation of certain silanol groups, which may condense and act as a barrier against further diffusion of ions inside and outside the glass [39,59,76]. However, according to [77], in glasses composed of $SiO_2{\cdot}R_2O$ and $SiO_2{\cdot}R_2O{\cdot}CaO$ with a high content of R_2O, the formed layer is not sufficient to

protect the glasses from rapid attack via de-alkalization or network dilution in the presence of aqueous acid solutions. In addition, some acids can attack calcium ions, giving rise to the formation of soluble complexes [78]; this attach could have occurred with the nitric acid used in this study. A relationship can be observed between the glasses obtained from the same wastes but in different proportions (G0.24, G0.36, and G0.39) and an increasing content of CaO (Fig. 9a): sample G0.39 presented the lowest chemical resistance because more than 50% of the sample mass was consumed after 2 h, but is likely due to a high solubility of akermanite in mineral diluted acids [59]. Whereas sample G0.24 presented the highest acid resistance, with a mass loss of less than 2%, due to anorthite content which are stable in acid medium [59].

In the case of glass ceramics, mass loss in the acidic environment (HNO_3) tended to increase as the CaO/SiO_2 ratio increased. Sample GC0.39 presented the highest loss (14%), whereas sample GC0.24 showed the highest acid resistance, with a maximum mass loss of 0.28%. It is important to highlight that, unlike glasses, the chemical stability of glass-ceramic materials is directly associated with the composition and amount of crystalline phases present [75]. Ref. [79] claimed that crystallization is the main factor that affects the chemical resistance of glass ceramics in acidic solutions because phases such as lithium metasilicate, disilicate, gehlenite and anorthite can coexist. These phases decompose in the presence of acid, negatively impacting the chemical resistance of the material. In contrast, quartz and a variety of pyroxene phases (e.g., wollastonite) and their solid solutions can improve the durability due to their high resistance to the action of acids (almost insoluble) [80,81]. The above results agree with the results of a study by Jordan [82], who claimed that, in acidic solutions, the formation of a leached layer of residual silica would seem unlikely in anorthite because Si—O—Si bridge bonds (siloxane) are almost absent.

During the attack of glass by alkaline solutions, the OH^- ion plays a determining role, interacting with the glassy matrix [24,39]. The breaking of the oxygen bonds leads to the formation of soluble silicate anions, causing progressive solubilization of the glass. The alkali and alkaline earth ions remain dissolved as long as they remain soluble; when they are no longer soluble, their hydroxides or respective carbonates precipitate [76]. After 6 h, sample G0.24 presented the highest mass loss of 4.5% in NaOH, followed by sample G0.39 with 2.8% and G0.36 with 1.4%, whereas the mass loss of the glass ceramics did not exceed 1% (Fig. 9a). The weight increase in samples G0.17 (Fig. 9b), G0.27 (Fig. 9c) and G0.37 (Fig. 9d) in the alkaline solution could be associated with the formation of an altered gel layer on the surface of the glass, which can also form upon exposure to alkaline solutions with a high pH, the formation of which is facilitated by the increased temperature of the experiment [76]. According to Maraghechi et al. [76], the presence of Ca^{2+} ions also has a significant impact on the dilution of glass because they can reduce the rate of material alteration either temporarily or permanently in high-pH, alkaline solutions due to the formation of a protective barrier layer that inhibits the dilution and transport of silicate ions. In general, the mass loss did not exceed 1 wt% and is considered very good. The authors found that a higher CaO/SiO_2 ratio favored the durability of glass ceramics [61].

Conclusions

The studies carried out in this research confirm the feasibility of implementing 100% Colombian waste of different origins as raw material to obtain low-cost glasses capable of immobilizing dangerous elements and transforming them into glass ceramics. The glass ceramics obtained possessed crystalline phases such as anorthite and wollastonite, which were expected on the basis of the $CaO—Al_2O_3—SiO_2$ system selected for the formulation of the mixtures. There was no evidence of a drastic influence of the CaO/SiO_2 molar ratio on the physical, chemical, and mechanical properties established; however, the Fe_2O_3 content influenced the crystallization process, as the samples that presented a content greater than 4% by weight did not produce exothermic DSC peaks corresponding to the crystallization temperature. Thus, it was not possible to obtain glass ceramics from frits F0.17 and F0.27 via heat treatment.

The glass-ceramic designs obtained had microhardness values of 612–701 MPa, fracture toughness values of 0.45–1.06 MPa $m^{1/2}$, friction coefficients μ of 0.57–1.0, and porosities of 0.18–5.7%, similar to the characteristics of standard materials used in the construction industry, such as natural stone, commercial glass ceramics, and even glazes for tiles and ceramics.

In general, all the compositions evaluated resulted in glasses with good chemical stability in NaOH solutions, since the mass loss of all samples did not exceed 5%. However, the glasses and glass ceramics developed in this study were more susceptible to HNO_3 attack. Sample GC0.24 presented the highest durability in the two environments evaluated (NaOH and HNO_3). All these findings indicate that the commercial use of glass ceramics obtained from Colombian industrial wastes without additives is very promising for monofired tiles production.

The glass ceramic with a molar ratio of 0.39 based on a mixture of 30 wt% FA, 30 wt% RV and 40 wt% GBFS presented the best mechanical performance (modulus of elasticity of 102 GPa, fracture toughness of 1.06 MPa $m^{1/2}$, and coefficient of friction of 1.0) and should be considered for potential application in the production of glazes for residential tiles. The glass ceramic with a 0.24 molar ratio had the highest durability and therefore high potential for applications in glazes for industrial tiles.

For future studies, a complete characterization involving analysis of the compressive strength, bending, dilatometry and thermal insulation of the glasses and glass ceramics produced in this study is recommended to better understand the mechanical behavior of these materials and expand their fields of application. Likewise, it is important to study the kinetic parameters of activation in glass ceramics using methods such as Kissinger's method and the Avrami or Johnson–Mehl–Avrami model, which determine the activation energy and the crystallization mechanism in samples without any prior knowledge of the reaction order, to further clarify the crystallization process.

Acknowledgments

The authors thank the Universidad del Valle for the financing received through the research projects, grant number C.I. 21025 and C.I. 2998. Additionally, they thank the Colombian companies that supplied the raw materials required for the investigation.

REFERENCES

[1] J.M. Rincón, Materias Primas para la Industria del Vidrio, in: M.Á. García, J.C. Cañaveras (Eds.), Utilización de rocas y minerales industriales, 2nd ed., 2005, pp. 49–74.
[2] R.K. Chinnam, A.A. Francis, J. Will, E. Bernardo, A.R. Boccaccini, Review. Functional glasses and glass-ceramics derived from iron rich waste and combination of industrial residues, J. Non-Cryst. Solids 365 (1) (2013) 63–74.
[3] W. Höland, G. Beall, Glass-Ceramic Technology, Second, John Wileys & Sons, 2012.
[4] R. Rawlings, J. Wu, A. Boccaccini, Glass-ceramics: their production from wastes – a review, J. Mater. Sci. 41 (3) (2006) 733–761.
[5] J. Dávalos, A. Bonilla, M.A. Villaquirán-Caicedo, R. Mejia de Gutiérrez, Preparation of glass–ceramic materials from coal ash and rice husk ash: Microstructural, physical and mechanical properties, Boletií la Soc. Española Cerámica y Vidr. (2020).
[6] J.M. Rincón, Vitreous and ceramic processing for the recycling of industrial wastes, Key Eng. Mater. 663 (October) (2016) 11–22.
[7] I. Ponsot, Glasses and glass-ceramic components from inorganic waste and novel processing, Universitá degli Studi di Padova (2015).
[8] L. Barbieri, A.M. Ferrari, I. Lancellotti, C. Leonelli, J.M. Rincón, M. Romero, Crystallization of (Na_2O–MgO)–CaO–Al_2O_3–SiO_2 glassy systems formulated from waste products, J. Am. Ceram. Soc. 83 (10) (2000) 2515–2520.
[9] Z. Yang, Q. Lin, S. Lu, Y. He, G. Liao, Y. Ke, Effect of CaO/SiO_2 ratio on the preparation and crystallization of glass-ceramics from copper slag, Ceram. Int. 40 (5) (2014) 7297–7305.
[10] D.I. Saparuddin, N.A.N. Hisham, S.A. Aziz, K.A. Matori, S. Honda, Y. Iwamoto, M.H.M. Zaid, Effect of sintering temperature on the crystal growth, microstructure and mechanical strength of foam glass-ceramic from waste materials, J Mater. Res. Technol. 9 (3) (2020) 5640–5647.
[11] A. Karamanov, M. Pelino, A. Hreglich, Sintered glass-ceramics from Municipal Solid Waste-incinerator fly ashes—Part I: The influence of the heating rate on the sinter-crystallisation, J. Eur. Ceram. Soc. 23 (6) (2003) 827–832.
[12] G.V. Sarrigani, I. Amiri, Literature review of glass-ceramic and willemite production from waste materials, in: Willemite-Based Glass Ceramic Doped by Different Percentage of Erbium Oxide and Sintered in Temperature of 500–1100 °C, Springer, Cham, 2019.
[13] A.A. Francis, R.D. Rawlings, R. Sweeney, A.R. Boccaccini, Processing of coal ash into glass ceramic products by powder technology and sintering, Glas. Technol. 43 (2) (2002) 58–62.
[14] L.M. Schabbach, F. Andreola, E. Karamanova, I. Lancellotti, A. Karamanov, L. Barbieri, Integrated approach to establish the sinter-crystallization ability of glasses from secondary raw material, J. Non-Cryst. Solids 357 (1) (2011) 10–17.
[15] D.M.A. Valderrama, J.A.G. Cuaspud, J.A. Roether, A.R. Boccaccini, Development and characterization of glass-ceramics from combinations of slag, fly ash, and glass cullet without adding nucleating agents, Materials (Basel) 12 (12) (2019).
[16] A.A. Francis, R.D. Rawlings, R. Sweeney, A.R. Boccaccini, Crystallization kinetic of glass particles prepared from a mixture of coal ash and soda-lime cullet glass, J. Non-Cryst. Solids 333 (2004) 187–193.
[17] I.K. Mihailova, P.R. Djambazki, D. Mehandjiev, The effect of the composition on the crystallization behavior of sintered glass-ceramics from blast furnace slag, Bulg. Chem. Commun. 43 (2) (2011) 293–300.
[18] Z. Wang, W. Ni, Y. Jia, L. Zhu, X. Huang, Crystallization behavior of glass ceramics prepared from the mixture of nickel slag, blast furnace slag and quartz sand, J. Non-Cryst. Solids 356 (31–32) (2010) 1554–1558.
[19] L. Barbieri, I. Lancellotti, T. Manfredini, G.C. Pellacani, J.M. Rincón, M. Romero, Nucleation and crystallization of new glasses from fly ash originating from thermal power plants, J. Am. Ceram. Soc. 58 (2001) 1851–1858.
[20] A.A. Francis, R.D. Rawlings, A.R. Boccaccini, Glass-ceramics from mixtures of coal ash and soda-lime glass by the petrurgic method, J. Mater. Sci. 21 (2002) 975–980.
[21] T.W. Cheng, T.H. Ueng, Y.S. Chen, J.P. Chiu, Production of glass-ceramic from incinerator fly ash, Ceram. Int. 28 (2002) 779–783.
[22] J. Luan, A. Li, T. Su, X. Cui, Synthesis of nucleated glass-ceramics using oil shale fly ash, J. Hazard. Mater. 173 (2010) 427–432.
[23] D. Hieu, K. Wang, J. Chen, B. Xuan, B. Hoang, Glass – Ceramic From Mixtures of Bottom Ash and Fly Ash, vol. 32, 2012, pp. 2306–2314.
[24] E. Montoya-Quesada, M.A. Villaquirán-Caicedo, R. Mejía de Gutiérrez, J. Muñoz-Saldaña, Effect of ZnO content on the physical, mechanical and chemical properties of glass-ceramics in the CaO–SiO_2-Al_2O_3 system, Ceram. Int. (2019, October).
[25] M. Kalirajan, R. Ranjeeth, R. Vinothan, S.M. Vidyavathy, N.R. Srinivasan, Influence of glass wastes on the microstructural evolution and crystallization kinetics of glass-ceramic glaze, Ceram. Int. 42 (16) (2016) 18724–18731.
[26] S.R. Teixeira, R.S. Magalhães, A. Arenales, A.E. Souza, M. Romero, J.M. Rincón, Valorization of sugarcane bagasse ash: producing glass-ceramic materials, J. Environ. Manage. 134 (2014) 15–19.
[27] Z. Yang, Q. Lin, J. Xia, Y. He, G. Liao, Y. Ke, Preparation and crystallization of glass-ceramics derived from iron-rich copper slag, J. Alloys Compd. 574 (2013) 354–360.
[28] World Energy Council, "World Energy Resources 2016," 2016.
[29] J.M. Mejía, E.D. Rodríguez, R. Mejía De Gutiérrez, Utilización potencial de una ceniza volante de baja calidad como fuente de aluminosilicatos en la producción de geopolímeros, Ing. y Univ. 18 (2) (2014) 309–327.
[30] H. Sánchez, Estado del arte sobre las escorias negras de horno de arco eléctrico y sus aplicaciones en pavimentos, L'esprit Ingénieux 7 (1) (2017) 1–14.
[31] H. Rondón, W. Fernández, D. Patiño, J. Ruge, H. Vacca, F. Reyes, Characterization of blast furnace slag for road projects, Rev. Ing. la Construcción 33 (1) (2018) 83–92.
[32] C. Zeynel, Global slag 2018 review, in: 13th Global Slag Conference, Exhibition & Awards, 2018, p. 2018.
[33] Y. Jani, W. Hogland, Waste glass in the production of cement and concrete – a review, J. Environ. Chem. Eng. 2 (3) (2014) 1767–1775.
[34] L. Barbieri, T. Manfredini, I. Queralt, J.M. Rincon, M. Romero, Vitrification of fly ash from thermal power stations, Glas. Technol. 38 (5) (1997) 165–170.
[35] B. Liu, Q.W. Yang, S.G. Zhang, Integrated utilization of municipal solid waste incineration fly ash and bottom ash

for preparation of foam glass–ceramics, Rare Met. 38 (10) (2019) 914–921.
[36] K. Das, S. Raha, D. Chakraborty, S. Burhanuddin, Saheb Ali, Effect of nucleating agents on the crystallization and microstructural characteristics of blast furnace slag derived glass-ceramics, Trans. Indian Ceram. Soc. 71 (3) (2012) 137–142.
[37] S. Çoruh, O.N. Ergun, T.W. Cheng, Treatment of copper industry waste and production of sintered glass-ceramic, Waste Manag. Res. 24 (3) (2006) 234–241.
[38] A. Karamanov, I. Gutzow, I. Chomakov, J. Christov, L. Kostov, Synthesis of wall-covering glass-ceramics from waste raw materials, Glas. Sci. Technol. Frankfurt 67 (8) (1994) 227–230.
[39] E. Cedillo, Síntesis y caracterización de materiales vitrocerámicos a partir de escorias metalúrgicas y su posible aplicación tecnológica, Universidad Autónoma de Nuevo León (2010).
[40] ASTM International, "ASTM C329-88 (2016) – Standard Test Method for Specific Gravity of Fired Ceramic Whiteware Materials," West Conshohocken, 2016.
[41] J. Shi, F. He, C. Ye, L. Hu, J. Xie, H. Yang, X. Liu, Preparation and characterization of $CaO–Al_2O_3–SiO_2$ glass-ceramics from molybdenum tailings, Mater. Chem. Phys. 197 (2017) 57–64.
[42] H. Isa, A review of glass-ceramics production from silicate wastes, Int. J. Phys. Sci. 6 (30) (2011) 6781–6790.
[43] S. Kucharczyk, M. Sitarz, M. Zajac, J. Deja, The effect of CaO/SiO(2) molar ratio of CaO–Al(2)O(3)–SiO(2) glasses on their structure and reactivity in alkali activated system, Spectrochim. Acta A. Mol. Biomol. Spectrosc. 194 (2018) 163–171.
[44] S. Wang, C. Zhang, J. Chen, Utilization of coal fly ash for the production of glass-ceramics with unique performances: a brief review, J. Mater. Sci. Technol. 30 (12) (2014) 1208–1212.
[45] S. Takahashi, D.R. Neuville, H. Takebe, Thermal properties, density and structure of percalcic and peraluminus $CaO–Al_2O_3–SiO_2$ glasses, J. Non-Cryst. Solids 411 (2015) 5–12.
[46] A.R. Alao, L. Yin, Nano-mechanical behaviour of lithium metasilicate glass-ceramic, J. Mech. Behav. Biomed. Mater. 49 (2015) 162–174.
[47] G.R. Anstis, P. Chantikul, B.R. Lawn, D.B. Marshall, A critical evaluation of indentation techniques for measuring fracture toughness: I, Direct crack measurements, J. Am. Ceram. Soc. 64 (9) (1981) 533–538.
[48] ASTM International, "G99-05 Standard Test Method for Wear Testing with a Pin-on-Disk Apparatus." West Conshohocken, PA, 2005.
[49] N. Effendy, Z. Abdul Wahab, H. Mohamed Kamari, K.A.S. Matori, Hj. Ab Aziz, M.H.M. Zaid, Structural and optical properties of Er^{3+} doped willemite glass-ceramics from waste materials, Optik (Stuttg) 127 (24) (2016) 11698–11705.
[50] A.S.T.M. International, Standard test method for density, absorption and voids in hardened concrete, ASTM C642-13 (2013).
[51] S.M. Marcus, R.L. Blaine, Thermal conductivity of polymers, glasses & ceramics by modulated DSC, Thermochim. Acta 243 (1994) 231–239.
[52] J. Deubener, M. Allix, M.J. Davis, A. Duran, T. Höche, T. Honma, T. Komatsu, S. Krüger, I. Mitra, R. Müller, S. Nakane, M.J. Pascual, J.W.P. Schmelzer, E.D. Zanotto, S. Zhou, Updated definition of glass-ceramics, J. Non-Cryst. Solids 501 (2018) 3–10.
[53] M.I. Martín, J.M. Rincón, F. Andreola, L. Barbieri, F. Bondioli, I. Lancellotti, M. Romero, Materiales vitrocerámicos del sistema $MgO–Al_2O_3–SiO_2$ a partir de ceniza de cáscara de arroz, Bol. la Soc. Esp. Ceram. y Vidr. 50 (4) (2011) 201–206.
[54] O.C. Mocioiu, I. Atkinson, J. Pandele, L. Boroica, B. Sava, A.M. Mocioiu, M. Zaharescu, Protective coatings for the silicate glasses containing Fe_2O_3, Rev. Roum. Chim. 59 (3–4) (2014) 267–272.
[55] M. Leśniak, J. Partyka, M. Sitarz, Influence of SiO_2/Al_2O_3 molar ratio on phase composition and surfaces quality of aluminum silicate sanitary glazes in the $SiO_2–Al_2O_3–CaO–Na_2O$ system, Arch. Metall. Mater. (4) (2016, December).
[56] M. Pal, S. Das, S.K. Das, Anorthite porcelain: synthesis, phase and microstructural evolution, Bull. Mater. Sci. 38 (2015) 551–555.
[57] L. Barbieri, A. Bonamartini, I. Lancellotti, Alkaline and alkaline-earth silicate glasses and glass-ceramics from municipal and industrial wastes, J. Eur. Ceram. Soc. 20 (2000) 2477–2483.
[58] J.M.G. Ventura, D.U. Tulyaganov, S. Agathopoulos, J.M.F. Ferreira, Sintering and crystallization of akermanite-based glass-ceramics, Mater. Lett. 60 (2006) 1488–1491.
[59] M. Romero, M.S. Hernández-Crespo, J.M. Rincón, Leaching behaviour of a glassy slag and derived glass ceramics from arc plasma vitrification of hospital wastes, Adv. Appl. Ceram. 108 (1) (2009) 67–71.
[60] M. Tarrago, M. Garcia-Valles, M.H. Aly, S. Martínez, Valorization of sludge from a wastewater treatment plant by glass-ceramic production, Ceram. Int. 43 (1) (2017) 930–937.
[61] H. Chen, B. Li, M. Zhao, X. Zhang, Y. Du, Y. Shi, J.S. McCloy, Lanthanum modification of crystalline phases and residual glass in augite glass ceramics produced with industrial solid wastes, J. Non-Cryst. Solids 524 (2019) 119638.
[62] D. Chicot, D. Mercier, F. Roudet, K. Silva, M.H. Staia, J. Lesage, Comparison of instrumented Knoop and Vickers hardness measurements on various soft materials and hard ceramics, J. Eur. Ceram. Soc. 27 (4) (2007) 1905–1911.
[63] S. Banijamali, B. Eftekhari Yekta, H.R. Rezaie, V.K. Marghussian, Crystallization and sintering characteristics of $CaO–Al_2O_3–SiO_2$ glasses in the presence of TiO_2, CaF_2 and ZrO_2, Thermochim. Acta 488 (1–2) (2009) 60–65.
[64] F. Pei, H. Guo, P. Li, B. Yan, J. Li, P. Yang, G. Zhu, Influence of low magnesia content on the $CaO–Al_2O_3–SiO_2$ glass-ceramics: Its crystallization behaviour, microstructure and physical properties, Ceram. Int. 44 (16) (2018) 20132–20139.
[65] R. Jia, L. Deng, F. Yun, H. Li, X. Zhang, X. Jia, Effects of SiO_2/CaO ratio on viscosity, structure, and mechanical properties of blast furnace slag glass ceramics, Mater. Chem. Phys. 233 (2019) 155–162.
[66] Y. Hou, G.-H. Zhang, K.-C. Chou, D. Fan, Effects of CaO/SiO_2 ratio and heat treatment parameters on the crystallization behavior, microstructure and properties of $SiO_2–CaO–Al_2O_3–Na_2O$ glass ceramics, J. Non-Cryst. Solids 538 (2020) 120023.
[67] A. Karamanov, M. Pelino, Induced crystallization porosity and properties of sintereds diopside and wollastonite glass-ceramics, J. Eur. Ceram. Soc. 28 (3) (2008) 555–562.
[68] G. Xia, L. He, D. Yang, Preparation and characterization of $CaO–Al_2O_3–SiO_2$ glass/fused silica composites for LTCC application, J. Alloys Compd. 531 (2012) 70–76.
[69] W.Y. Zhang, H. Gao, Y. Xu, Sintering and reactive crystal growth of diopside-albite glass-ceramics from waste glass, J. Eur. Ceram. Soc. 31 (9) (2011) 1669–1675.
[70] V. Fuertes, M.J. Cabrera, J. Seores, D. Muñoz, J.F. Fernández, E. Enríquez, Enhanced wear resistance of engineered glass-ceramic by nanostructured self-lubrication, Mater. Des. 168 (2019), 107623.
[71] G.G. Santos, F.C. Serbena, V.M. Fokin, E.D. Zanotto, Microstructure and mechanical properties of nucleant-free $Li_2O–CaO–SiO_2$ glass-ceramics, Acta Mater. 130 (2017) 347–360.

[72] E.I. Suzdal'tsev, Investigation of the strength and elastic properties of glass-ceramic of a lithium alumosilicate composition, J. Eng. Phys. Thermophys. 75 (2) (2002) 416–423.
[73] E. Bernardo, E. Bonomo, A. Dattoli, Optimisation of sintered glass–ceramics from an industrial waste glass, Ceram. Int. 36 (5) (2010) 1675–1680.
[74] E. Nicoleau, F. Angeli, S. Schuller, T. Charpentier, P. Jollivet, M. Moskura, Rare-earth silicate crystallization in borosilicate glasses: effect on structural and chemical durability properties, J. Non-Cryst. Solids 438 (2016) 37–48.
[75] Z. Zhang, L. Zhang, A. Li, Development of a sintering process for recycling oil shale fly ash and municipal solid waste incineration bottom ash into glass ceramic composite, Waste Manag. 38 (2015) 185–193.
[76] H. Maraghechi, F. Rajabipour, C.G. Pantano, W.D. Burgos, Effect of calcium on dissolution and precipitation reactions of amorphous silica at high alkalinity, Cem. Concr. Res. 87 (2016) 1–13.
[77] J.A. Hernández, J.L. Oteo, Reacciones de la superficie del vidrio con soluciones acuosas, Bol. la Soc. Esp. Ceram. y Vidr. 21 (2) (1978) 81–98.
[78] J. Fernández-Navarro, A. Durán-Carrera, Tratamientos de la superficie de vidrio, Bol. la Soc. Esp. Ceram. y Vidr. 24 (5) (1985) 299–314.
[79] W. Deng, J. Cheng, P. Tian, M. Wang, Chemical durability and weathering resistance of canasite based glass and glass-ceramics, J. Non-Cryst. Solids 358 (21) (2012) 2847–2854.
[80] J. Kang, J. Wang, X. Zhou, J. Yuan, Y. Hou, S. Qian, S. Li, Y. Yue, Effects of alkali metal oxides on crystallization behavior and acid corrosion resistance of cordierite-based glass-ceramics, J. Non-Cryst. Solids 481 (2018) 184–190.
[81] J.L. Pérez, S. Reverter, E. Bou, A. Moreno, M.J. Vicente, A. Barba, Vidriados mates de alta temperatura con elevada resistencia química, Quailicer (2006) 179–194.
[82] K.G.K.G. Jordan, S.R. Higgins, C.M. Eggleston, S.M. Swapp, D.E. Janney, Acidic dissolution of plagioclase: in-situ observations by hydrothermal atomic force microscopy, Geochim. Cosmochim. Acta 63 (1999) 3183–3319.